



Machinability investigations through novel controlled flushing characteristics in wire electric discharge machining of M42 high-speed steel

Sana Ehsan¹ · Mudassar Rehman^{1,2} · Mohammad Pervez Mughal³ · Muhammad Umar Farooq⁴ · Muhammad Asad Ali¹

Received: 9 August 2021 / Accepted: 19 January 2022 / Published online: 12 February 2022
© The Author(s), under exclusive licence to Springer-Verlag London Ltd., part of Springer Nature 2022

Abstract

The industry anticipates technological advancements for productivity improvement, and this can be accomplished by improving the machining performance in the areas where machinability challenges exist. The machinability and productivity of wire electric discharge machining (WEDM), which is a popular non-conventional cutting process, can be improved while having comparable surface integrity. Previously the non-conventional machining literature is focused on the machinability investigations of various industrial materials and process optimization. However, no extensive research on the study of flushing parameters optimization to improve machinability in non-conventional machining is known. In this research, WEDM of M42 HSS using controlled flushing is performed resulting in improved machinability in terms of material removal rate (MRR), surface roughness (Ra), and kerf width (KW). The findings indicate that the nozzle diameter (76.85%) has a substantial influence on total machining performance. Nozzle diameter, nozzle-workpiece distance, servo voltage, and flushing pressure all had a substantial influence on MRR, with percentage contributions of 34.50%, 26.02%, 22.94%, and 14.21%, respectively. Furthermore, multi-response optimization is also performed and depicts the possibility of achieving optimized values of MRR, Ra, and KW simultaneously. The flush-controlled machining improved work quality in terms of accurate production, increased productivity by lowering process time, and improved surface integrity of the machined piece thus can be a possible process advancement in the aerospace and automotive industries.

Keywords Wire electric discharge machining (WEDM) · Controlled flushing · Machinability investigation · Material removal rate · Surface roughness · Kerf width

1 Introduction

Productivity increase is always sought to reduce the production cost and to gain a competitive advantage. The ongoing technological advancements and high-speed machining can be a potential solution for the mechanical industry [1]. High-speed steel (HSS) has greater mechanical qualities, a higher hardness, better shock resistance, better fracture toughness, and exceptional fatigue resistance [2]. As a result, HSS finds its applications in hard rotating and cutting tools, forging, and stamping dies [3]. The machinability investigation of high hardness materials like Ti alloys, Inconel 718, and HSS with complex shapes has always been a challenge by using conventional machining processes like turning, milling, and drilling. This is due to fact that these processes find it difficult if not impossible to machine the hard materials with complex profiles/geometries. Non-conventional

✉ Mudassar Rehman
mudassar@mail.nwpu.edu.cn

✉ Muhammad Umar Farooq
umarmuf0@gmail.com

¹ Department of Industrial and Manufacturing Engineering, University of Engineering and Technology, Lahore 54890, Pakistan

² Industry Engineering Department, School of Mechanical Engineering, Northwestern Polytechnical University, Xian 710072, China

³ Industrial Engineering Department, University of Management and Technology, Lahore, Pakistan

⁴ School of Mechanical Engineering, University of Leeds, LS2 9JT Leeds, UK

machining can be an effective solution to cope with the said issues. M42 HSS is widely used in aerospace and machining industries for making high-speed moving parts like turbine blades, moving cutters, and different machining tools through wire electric discharge machining (WEDM). The prime challenges like process stability, productivity, and surface integrity have become the main concerns while fabricating moving parts. These said issues must be controlled and monitored to attain higher machining efficiency. Also, the flushing characteristics including flushing pressure, flushing nozzle diameter, and flushing nozzle workpiece distance, have become an inevitable concern these days to make a balance among the machining productivity and process stability, along with the dimensional accuracy of the machined parts.

Different non-conventional machining techniques like electro-chemical machining, laser-assisted machining, plasma arc cutting, electron beam machining, water/abrasive water jet machining, and electro-discharge machining, can be employed to generate complex profiles in hard/difficult to machine materials. Wire electric discharge machining (WEDM) is a competitive non-traditional process to deal with a variety of conductive materials. WEDM is a specialized thermal electro-sparks erosion process capable of accurately machine the part with varying hardness and complex shapes [26]. An increase in redeposition of debris during machining results in poor surface finish, dimensional errors, and recast layer thickness [4–6]. Therefore, parametric optimization is required to enhance the MRR, reduce Ra, recast layer, dimensional deviation, and Kw.

Controlled-flushing involving the careful flushing characteristics plays a crucial role in the machining performance in WEDM during electro-sparks erosion. Thus, the machinability in EDM can be enhanced by the parametric investigation of flushing pressure (Pf), flushing nozzle diameter (Dn), and the flushing nozzle to workpiece distance (d) [7–9]. Optimized dielectric flushing not only affects the processing speed but also the quality of the machined surface. A too high value of Pf reduces the machining speed, whereas the 'd' and 'Dn' increase the wire vibrations and thus wire lag (WL) phenomenon which adversely influence the dimensional accuracy of the machined workpiece. Therefore, the WL should be minimized to attain higher machining efficiency. An optimized combination of flushing characteristics reduces the WL as expressed by Chakraborty et al. [7]. It is known that an increase in Pf and wire tension (WT) enhance the machinability and dimensional accuracy. The electrical parameters like fine finish power supply, pulse width, servo voltage, and pulse current also contribute a key role in enhancing the machining performance while improved removal of debris is important for stable machining [27, 28].

The machinability investigation in EDM is performed in various research works to examine the influence of different

physical, electrical, and process variables for increased performance accuracy. Rehman et al. [10] concluded that Pf influenced a lot in controlling the amount of machined debris along with cooling of the workpiece and wire electrode. It was further explained that the Pf significantly increased the dimensional accuracy with an error reduction in cylindricity (49.5%), diametral (37.84%), and circularity (31.02%), respectively. Qudeiri et al. [5] examined the effect of variation in Vs, Pon, WT, and Ip on wear performance in WEDM of 316L stainless steel and resulted in the higher influence of Pon and Ip on wear behavior for die making industries. It was also inferred that the increase in discharge energy during machining increases the redeposition of debris, oxide formation, and craters which alleviated the wear resistance and micro-hardness of the machined workpiece. Singh et al. [11] investigated the influence of pulse peak current (Ip), pulse duration (Pon), and wire feed (WF) on machining speed in WEDM of Inconel 718. It was inferred that the processing speed is significantly influenced by Pon with a 74.91% contribution percentage. Similar results were reported by Camposeco-Negrete [12] when performing WEDM of DC53 steel. It was further explained that the size and density of craters' formation are highly dependent on the sparks' discharge energy during machining. Straka and Dittrich [13] carried an experimental study in WEDM of HSS and concluded that the control variables like Pon and pulse off (Poff) are highly influenced on the dimensional accuracy to improve the machining performance. Sanke [14] examined the influence of control variables in WEDM of Al composite and concluded that the performance efficiency concerning the MRR can be improved by optimizing the duration of the spark (Pon and Poff). Ar et al. [15] reported the higher influence of Vs and Poff in reducing the machining cycle time (7.50%) and Ra (1.16%) in WEDM of O1 tool steel. It was further concluded that the SR is also highly influenced by the variations in pulse-off duration. Kumar et al. [16] concluded that the physical properties and chemical composition of the machined workpiece in WEDM are highly influenced by the surface quality in terms of Ra. Mathematical models were also developed to determine a suitable combination of electrical conductivity of the workpiece (98.41%) and the Ip (95.02%).

Indeed, several works are available on machinability investigation using various engineering materials in wire electric discharge machining. However, little works are available on the investigation of flushing characteristics for to enhance the machinability. Furthermore, the multi-response optimization of controlled flushing was not explicitly discussed, which is the core of the work reported herein. Three key flushing variables namely flushing pressure, flushing nozzle diameter, and the nozzle-workpiece distance along with one electrical parameter known as servo voltage were investigated under L18 Taguchi experimental design. Material removal rate, surface roughness, and kerf width are the defined responses. The statistical analyses

Table 1 Elemental composition and characteristics of M type HSS [29]

Name	Unit	Value
Modulus of elasticity	GPa	207
Ultimate tensile strength (UTS)	MPa	800
Machinability (1% carbon steel)	%	65
Hardness	HRC	64.3
Thermal conductivity	W/m–K	41,5
Poisson ratio	v	0.27

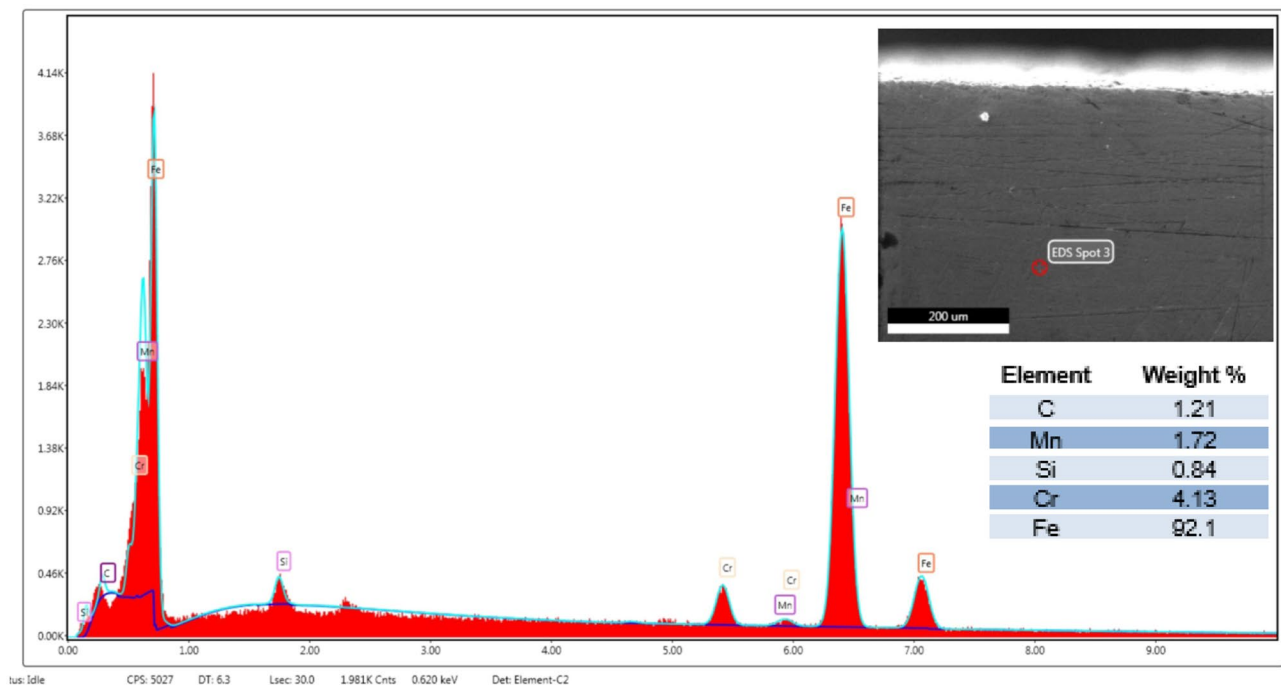
include main effects, regression-based variance analysis, Pareto charts, and normal plots. Optical microscopy and scanning electron microscopy were also carried to investigate the surface morphology and recast layer thickness (RLT) in a detailed manner. Parametric single-objective and multi-objective optimization are carried out to facilitate machinists in decision-making for controlled lubrication to enhance machinability. The novelty of the work lies in the investigation of machining stability, productivity, and surface integrity via optimized flushing parameters for WEDM of M42 HSS that are equally applicable to other materials.

2 Materials and methods

M42 grade high-speed steel (HSS) that finds its applications in various engineering industries, was chosen as the workpiece material in this study. The density and the dimensions of the workpiece were taken as $7.972 \times 10^3 \text{ kg/m}^3$ and

3 cm 20 cm*3 cm. HSS possesses high hot hardness, high self-hardening ability, higher fracture toughness, improved shock, and fatigue resistance [17]. The technical details of the work material are reported in Table 1 and EDX-based chemical specifications are indicated in Fig. 1. Experimentation was performed using CNC submerged wire EDM (CHMER G43S) with de-ionized water dielectric including zeolite as a de-ionizing agent. The hard type of brass wire (with tensile strength around 900 MPa) and diameter (0.25 mm) was chosen as a tool electrode. The detailed demonstration of the experimental setup is shown in Fig. 2.

Both the workpiece and wire electrode were completely dipped in the di-electric fluid throughout the machining process. The electrode wire was threaded by an automatic wire threaded mechanism between the upper and lower nozzles. The pressure of dielectric (Pf) can be varied by using the adjusting knobs as illustrated in Fig. 2. The distance between the workpiece and the flushing nozzle can also be changed by using the manual pulse generator of the CNC wire EDM. The electrode wire was passed through the workpiece during the machining operation to produce a machined slot/kerf in the workpiece as can be seen in Fig. 3. Three different sized flushing nozzles were employed in the experimentation. The dielectric fluid was flushed from the upper and lower nozzles during electro-sparks erosion. Vs controls the wire retracts, advancement, and the distance between the wire electrode and the workpiece. Therefore, the control variables in this study include Pf, Dn, d, and Vs.

**Fig. 1** EDX analysis of the machined surface indicating the chemical composition of the workpiece material(HSS)

The machining performance concerning the cutting speed was observed directly from the WEDM monitor display screen and MRR was calculated from the relationship reported in Eq. (1).

$$MRR(\text{mm}^3/\text{min}) = \left[\frac{Ma - Mb}{Tm * \rho} \right] \tag{1}$$

where “*Ma*” and “*Mb*” denoted the mass before and after the machining cycle. “*Tm*” symbolized the cycle time, and “*ρ*” indicated the material density.

A surface texture meter (Surtronic 128) was used to assess the machined Ra at an evaluation length of 4 mm and a cut-off length of 0.8 mm. After measuring roughness at five distinct locations on the machined surface in terms of arithmetic average roughness, the standard deviation for all of the data was calculated for each experiment. Because the standard deviation in all of the roughness experimental data is quite small, the average value was presented here.

KW was measured using coordinate measuring equipment (Chen Wei CE-450DV). On the machined slot, three measurements were recorded for investigation purposes. A detailed statistical analysis was performed for deep insight to comprehend the influence of flushing characteristics on the said output responses. The process variables with their levels, output responses, and constant factors during machining are reported in Table 2. Figure 4 represents the current research plan and methodology.

3 Results and discussions

The machining results were obtained by performing experiments following the Taguchi L_{18} array as mentioned in Table 3. The evaluation of output responses resulted in an increased MRR (21.99 mm³/min), along with reduced Ra (1.90 μm), and Kw (0.354 mm), respectively. Higher levels of “Pf” and “d” are observed to enhance the machining performance in terms of improved MRR and surface finish. The rationale of this improvement is the easy evacuation of debris particles from the working regime. The specific discussions about the study results are comprehensively elaborated in the forthcoming sections.

3.1 Analysis of parametric effects

Main effects plots are usually employed to visualize the direct parametric variations for output responses. Therefore, it is quite easy to optimize the process physics after a detailed understanding of the parametric trends. The details of the graphical illustrations for MRR, Ra, and KW are comprehensively discussed in the forthcoming sections.

3.1.1 Parametric trends analysis for material removal rate (MRR)

The analysis of parametric effects from Fig. 5 has indicated that the MRR was linearly enhanced by increasing the levels of Vs, Pf, and d, whereas Dn behaved inversely with it. This is due to more area of the heat-affected zone (HAZ) at increased Vs and d resulting in more melting and vaporization of debris. The dielectric flushing was improved by increasing the Pf, thus resulted in stable machining with minimal process fluctuations. The effects of each process variable on the set response are also explained onward in detail.

The Vs is in charge of keeping a safe distance among the two electrodes for uniform sparks discharges and avoiding short-circuiting for stable machining. The rise in Vs resulted in an acceptable quantity of discharge energy among the inter-electrodes gap, to promote the sufficiently melting and vaporization of work material. An increase in MRR from 17.2 mm³/min to 18.7 mm³/min was faced by increasing the Vs from level 1 (40 V) to level 2 (50 V) as evidenced in Fig. 5. It is because high discharge energy pulses were augmented by increasing the Vs in the machining regime required for the machining action to melt and vaporize the material. As a result, the intensity of sparks discharges is increased producing more debris; thus, recast layer appears on the machined surface as evidenced by the SEM image shown in Fig. 6. A higher Vs setting usually results in more electric pulses and more spark energy. The proper melting and vaporization of the workpiece material are ensured by the development of an acceptable quantity of spark energy in the workpiece electrode gap. As a result, the machining action is carried and the required results are obtained. More thermally affected region/HAZ is produced by increasing Vs; however, the density of sparks discharges required to

Table 2 Process parameters and constant factors

Parameters	Vs	Pf	Dn	d	Constant factors	
Units	V	kg/cm ²	mm	mm	Gap voltage (V)	90
L1	40	4	4	3	Pon (μs)	4
L2	50	8	6	10	Poff (μs)	30
L3	–	12	8	24	Electrode brass wire diameter (mm)	0.25

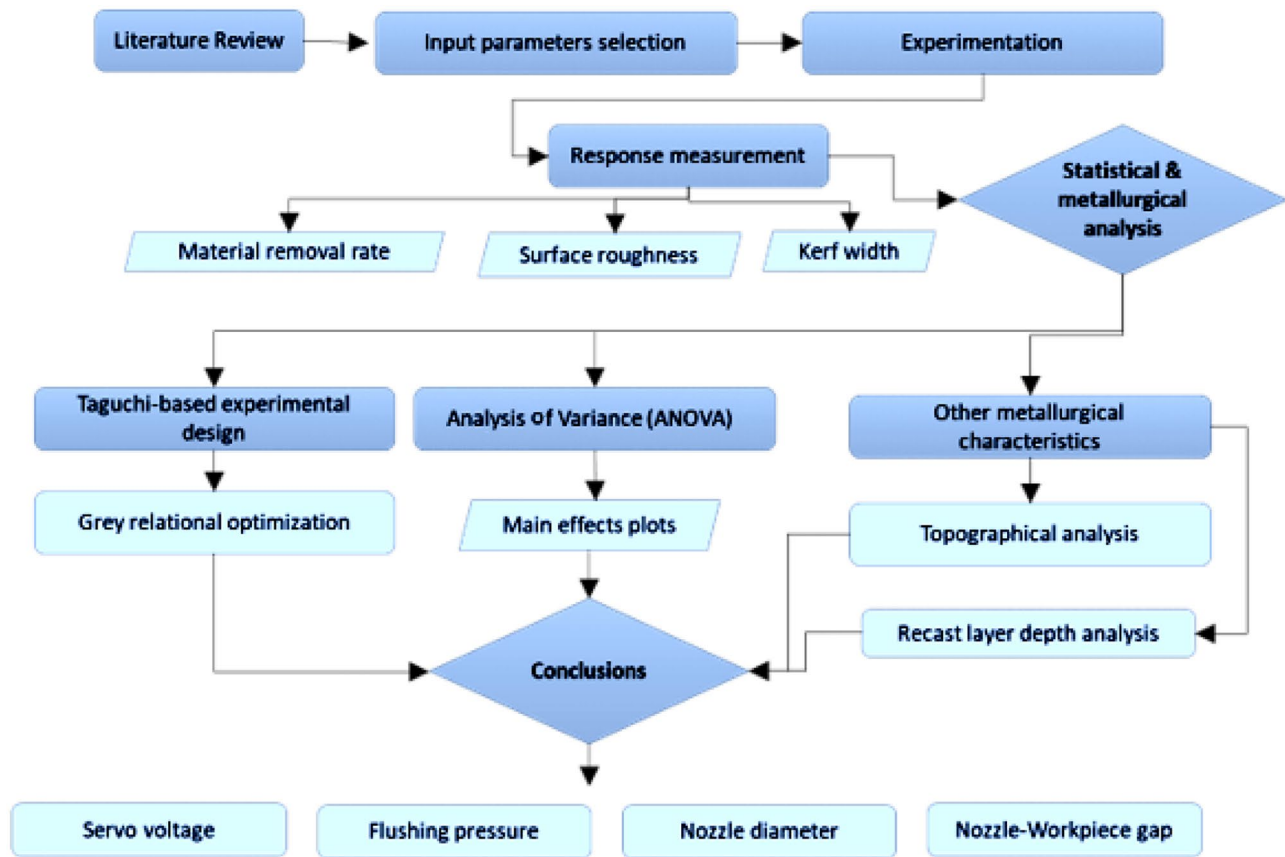


Fig. 4 Research plan and methodology

erode the workpiece is consequently reduced and similar findings were reported by Patel Gowdru Chandrashekarappa et al. [18].

Generally, two kinds of forces are produced during the dielectric flushing in EDM; one is the electro-erosive force which is generated because of the occurrence of discrete electric sparking, whereas the other force is produced due to the moving wire electrode because of injected dielectric through the flushing nozzles. The Pf plays an important role in influencing the machining productivity concerning MRR. A linear increase in MRR was observed from 16.2 mm³/min to 21.99 mm³/min by increasing the Pf from level 1 (4 kg/cm²) to level 3 (12 kg/cm²) as can be seen from Fig. 5. Actually, at 12 kg/cm², the kinetic energy of the injected flushing dielectric is notably higher, so it applies strong electro-erosive erosion to enhance the removal of the machined material. This strong flushing leads to more debris evacuation on the workpiece surface as shown in SEM images in Fig. 6. Thus, the controlled flushing uniforms the electro-discharge erosion and it can further enhance the MRR by increasing the Pf or by using low viscosity dielectric say kerosene over deionized water [19, 20]. The increased Pf also enhances the cooling phenomenon just after the thermal erosion of the workpiece.

The flushing nozzle diameter also plays its part in influencing MRR. According to the equation of continuity for the fluids, the less is the orifice area, the more will be the flushing speed. Therefore, a linear decrease in MRR was obtained from 21.9 mm³/min to 16.2 mm³/min by increasing the Dn from level 1 (4 mm) to level 3 (8 mm). It strongly infers that the nozzle with a smaller diameter will tend to enhance more localized erosion of the workpiece material with more flushing speed thus more kinetic energy of the flushing dielectric. This reduction in the intensity of dielectric flushing caused more molten material redeposited on the machined surface, thus greater-sized globules of debris on the machined surface. The effect of nozzle orifice opening diameter on the flushing intensity can also be seen in Fig. 7 for controlled flushing.

The controlled distance between the flushing nozzle and the workpiece is also an important aspect for machining performance investigation in terms of MRR. The “d” behaved linearly with MRR from level 1 (3 mm) to level 3 (24 mm) and tends to increase it from 16.2 mm³/min to 21.9 mm³/min. The rationale is the more area covered by the plasma pool consisting of electrons and ions thus produced more thermal damages on the work surface. However, an

Table 3 Design of experiments along with output results

Control variables					Output responses		
Exp. No.	Servo voltage	Flushing pressure	Nozzle diameter	Nozzle-workpiece gap	Material removal rate	Surface roughness	Kerf width
Symbol	Vs	Pf	Dn	d	MRR	Ra	KW
Unit	Volt	kg/cm ²	mm	mm	mm ³ /min	μm	mm
1	40	4	4	3	16.50	2.01	0.354
2	40	4	6	10	16.10	2.02	0.356
3	40	4	8	24	16.20	2.06	0.360
4	40	8	4	3	17.50	1.93	0.354
5	40	8	6	10	17.20	1.96	0.355
6	40	8	8	24	17.25	2.00	0.362
7	40	12	4	10	18.70	1.90	0.358
8	40	12	6	24	18.90	1.93	0.363
9	40	12	8	3	16.20	2.00	0.357
10	50	4	4	24	20.60	1.99	0.360
11	50	4	6	3	17.40	2.09	0.354
12	50	4	8	10	16.30	2.12	0.359
13	50	8	4	10	19.30	1.96	0.359
14	50	8	6	24	19.80	2.00	0.365
15	50	8	8	3	17.00	2.08	0.359
16	50	12	4	24	21.90	1.93	0.366
17	50	12	6	3	18.70	2.00	0.361
18	50	12	8	10	17.60	2.02	0.363

excessive increase in the electrodes gap caused the reduction in sparks intensity and thus reduces MRR. Therefore, the formation of minor redeposits on the machined surface is attributed to the reduction in plasma intensity as evidenced in the previous SEM image in Fig. 6.

3.1.2 Parametric trends analysis for surface roughness (Ra)

Surface roughness (Ra) usually denotes the measurement of surface discrepancies on the machined surface following the electro-sparks erosion. The Ra is caused by various

Fig. 5 Graphical illustration to indicate the parametric influence of control variables for MRR

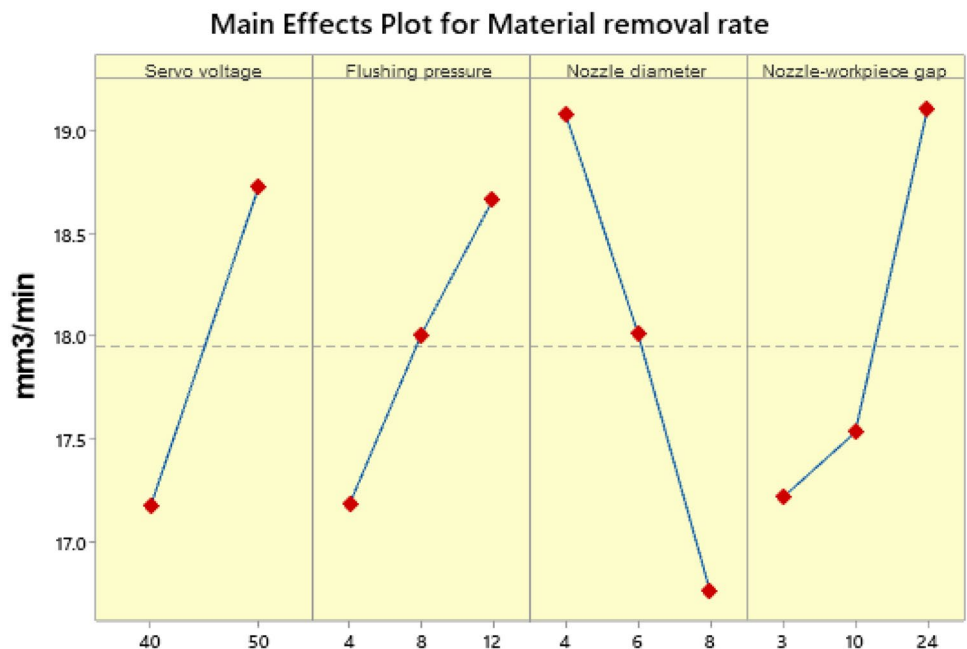
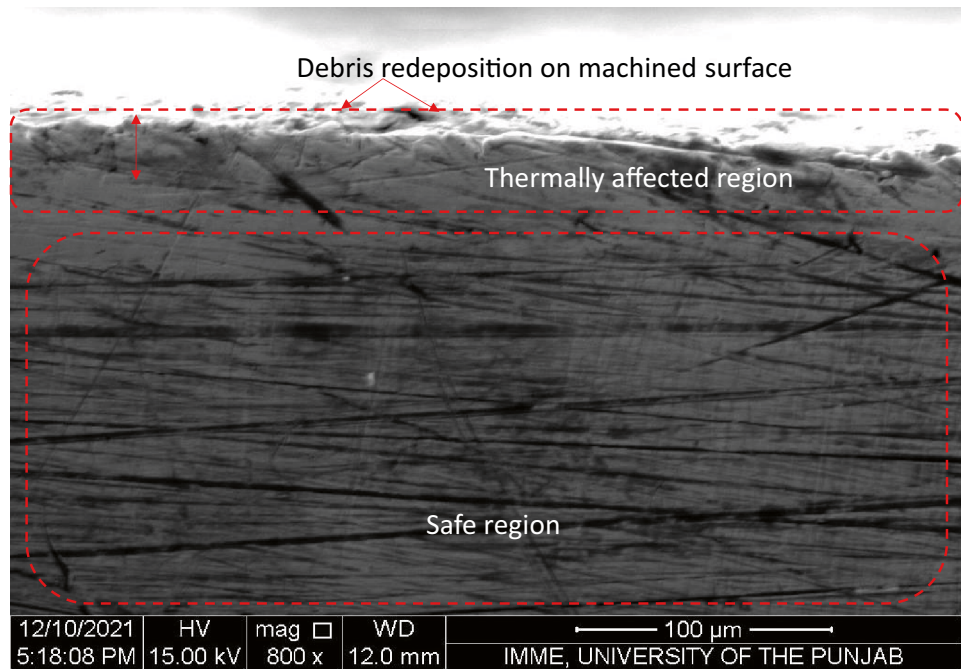


Fig. 6 SEM image to indicate the formation of the recast layer on the machined workpiece surface for 15th Exp



factors like poor dielectric flushing, enhanced width of HAZ, increased pulse duration, or the greater intensity of spark discharges. The parametric trends from Fig. 8 indicated that Vs and Dn vary directly, whereas Pf and d behaved inversely with Ra. The effect of each control variable for Ra is comprehensively explored in the upcoming sections.

As Vs was increased from level 1 (40 V) to level 2 (50 V), a linear increase in Ra was observed, as indicated in Fig. 8. The rationale for this increase is the enhanced voltage gap which increases the HAZ, resulting in formation of more debris redeposition, craters, and micro-cracks. This is also occurred by the considerable heat flux intensity transfer to the working regime, which is the primary cause of material erosion in EDM. A linear decrease in Ra from 2.12 μm to 1.92 μm was observed by increasing the Pf from level 1 (4 kg/cm^2) to level 3 (12 kg/cm^2). The rationale of this happening is quite evident as the strong Pf promotes the

rapid evacuation of the material, smaller craters, and surface asperities formed on the machined work surface as shown in the optical microscopic image in Fig. 10. The increased flushing pressure uniform the electro-discharge erosion and removes the debris particles at a faster rate. The flushing action in WEDM is schematically demonstrated in Fig. 9.

The Ra deteriorated from 1.90 μm to 2.02 μm with the increase of Dn from 4 to 8 mm as evidenced in the main effects plot from Fig. 8. It is due to fact that the intensity of the dielectric fluid is reduced according to the basic liquid flow principle resulting in the poor evacuation of melted debris, thus increased the Ra on the machined surface. This effect has also been visualized in the optical microscopic image in Fig. 10. A controlled distance/gap is required among the tool electrodes for sufficient melting and evacuation of the melted material. Thus, the nozzle workpiece distance behaved inversely with the Ra. The Ra is reduced from 2.02 μm to 1.90 μm as d is increased from 3 to 24 mm. The said behavior is obvious because of the reduction in the intensity of the spark for the erosion of the workpiece material.

Surface topography plays a crucial role to investigate the machined surface quality. Therefore, the effects of process parameters on the workpiece surface are studied using SEM and optical microscopic images. The effects show that surface characteristics (redeposited debris, cracks, craters, micro-pores) are closely related to the discharge energy phenomenon (electro-sparks erosion) that occurred during the process (see Figs. 6 and 10). This phenomenon is determined by nozzle-workpiece gap value such as high discharge energy (DE) tending to remove the material with

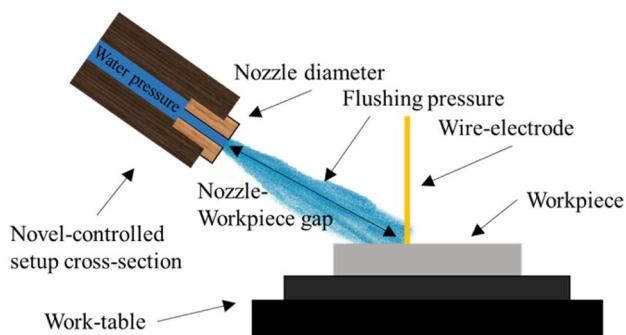
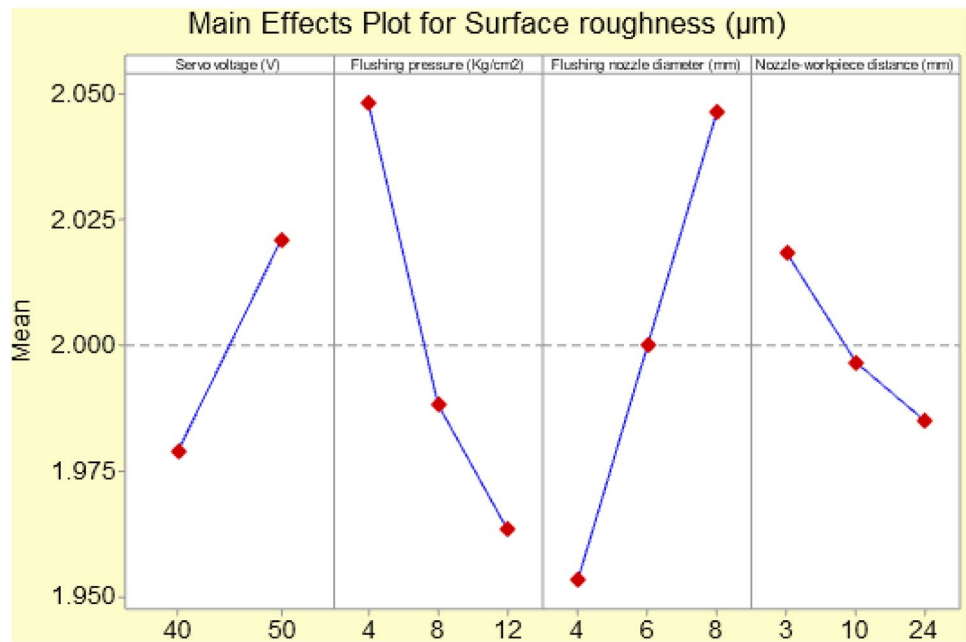


Fig. 7 Novel controlled flushing setup for WEDM to enhance the machinability

Fig. 8 Graphical illustration to indicate the parametric influence of control variables for Ra



high temperature through rigorous melting and vaporization on a localized area. With each intense discharge, deeper craters are formed and the ridge-rich surface is generated. It has been observed that machined surfaces contained

micro-pores, debris, and cracks craters due to successive discharges. The control over surface defects is very important to control internal crack propagation which is a potential cause of product failure.

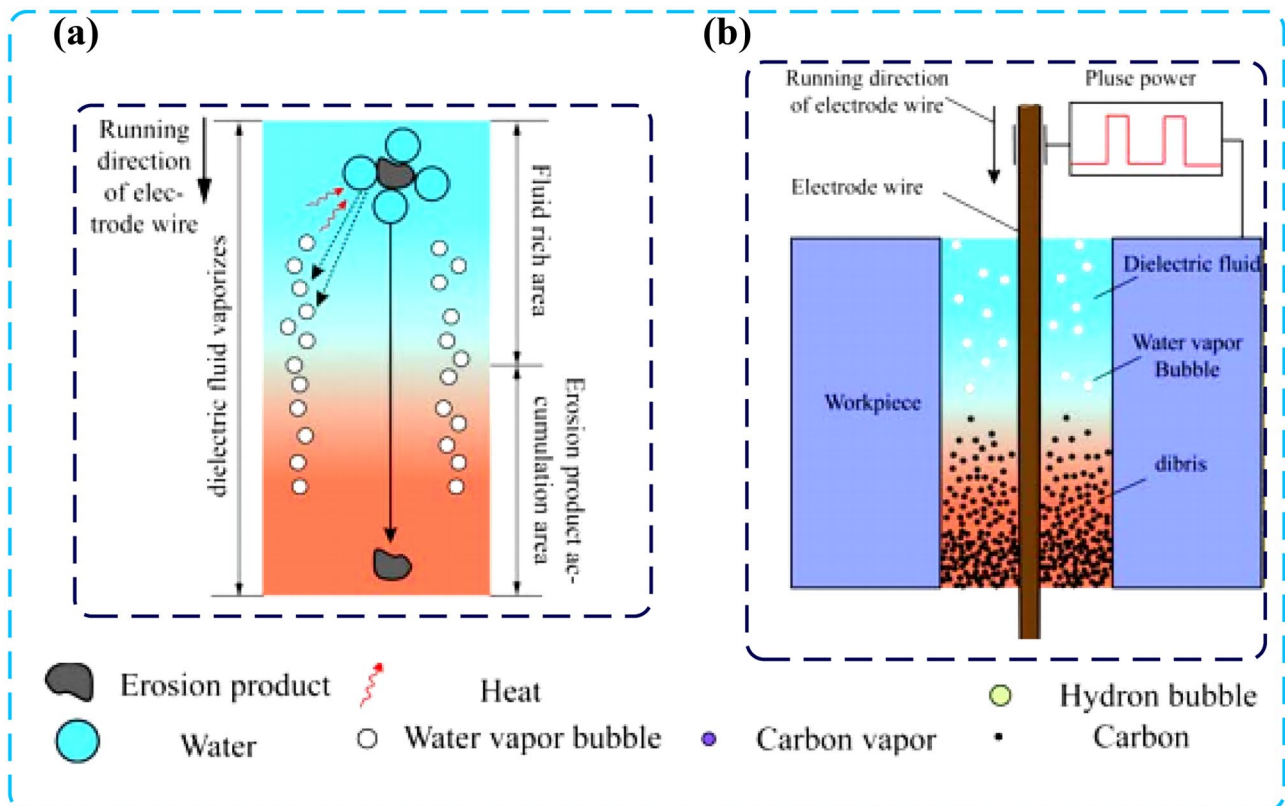


Fig. 9 Flushing action (a) interpole flushing mechanism, (b) holistic flushing control mechanism and its effects on machining (copyrighted and reprint permissions taken) [19]

During WEDM, cooling is essentially due to vaporization of dielectric fluid. However, there is a possibility of establishment of a vapor film on the wire and the workpiece that reduces the subsequent cooling and dryout condition as vapor film prohibits liquid to reach the wire and acts as an insulated layer. To increase cooling, vapor layer thickness should be minimized if cannot be eliminated. This may be achieved by increasing the pressure and velocity of dielectric through the nozzles. Therefore, higher mobility of lubrication is required to cool the interaction area for better flushing of debris [20]. As is evident from Fig. 9b, the erosion products produced by the discharge cannot be removed in time due to the lack of working fluid at lower Pf or high workpiece-nozzle gap, causing the inter-electrode erosion products to accumulate. The accumulation area is increased, the inter-electrode discharge state deteriorates, and the surface burn of the workpiece is severe. The micrographs, presented in Fig. 10, show surface morphology of cross-section representing the results of low discharge energy on the parameter's combination, which leads towards decreasing the recast depth to fabricate accurate dimensions of profile and better surface characteristics [21]. As the Pf decreases in Fig. 10, the debris accumulates and makes a recast layer on the surface. Minimization of the distance between the nozzle and required geometry machining area helps in adequate melting at the surface and proper flushing of debris.

The micrographs are taken to analyze the recast layer thickness (RLT) formed at the machined surface for 5th experimental test Vs (40 V), Pf (8 kg/cm²), Dn (6 mm), and d (10 mm) and 12th experimental test Vs (50 V), Pf (4 kg/cm²), Dn (8 mm), and d (10 mm) as shown in Fig. 10a, b. Recast layer was measured at three different places on the machined surface and the average was considered the final result for investigation. Figure 10 depicts that minimum RLT was observed at Vs = 40 V, Pf = 8 kg/cm², Dn = 6 mm, and d = 10 mm. The reason is that the redeposition of debris is declined as the spark's intensity was low, while the Pf was high. It was inferred that the maximum RLT was obtained at the maximum Vs (50 V), low level of Pf (4 kg/cm²), Dn (8 mm), and d (10 mm). RLT was found maximum because the spark intensity was high at high Vs and flushing pressure was low due to which maximum debris was deposited at the machined surface.

Severe effects of high Vs are observed on the surface due to high pulse on time which prolongs the spark duration. High discharge energy causes more melting through deeper and wider craters. High crack density and melt redeposits are formed on the surface, which is an indicator of more discharge energy transfer. It is evident from the surface analysis that the electro-sparks erosion phenomenon drives the surface characteristics. The spark produced against Fig. 10a is more intense in comparison to the spark generated in Fig. 10b.

Severe effects of high Vs are observed on the surface due to high pulse on time which prolongs the spark duration. High discharge energy causes more melting through deeper and wider craters. High crack density and melt redeposits are formed on the surface, which is an indicator of more discharge energy transfer. It is evident from the surface analysis that the electro-sparks erosion phenomenon drives the surface characteristics. The spark produced against Fig. 10a is more intense in comparison to the spark generated in Fig. 10b.

3.1.3 Parametric trends analysis for kerf width (KW)

Kerf width denotes the measurement of excessive material removed along the sides of the workpiece. Usually, the reduction in Kw is required as cannot be eliminated during electro-sparks erosion. The main effects plots for kerf width (Kw) are shown in Fig. 11 which demonstrates a direct linear relationship of all control variables with it. The effects of process parameters along with strong rationales for the set response are explained in the upcoming sections.

A linear increase in the KW was observed as Vs was increased from level 1 (40 V) to level 2 (50 V) as obvious from Fig. 11. The rationale of this increase is the enhanced thermally affected zone caused by increasing the gap voltage which removes extra material from both sides of the machined workpiece. This results in an increased spark gap for the erosion of the work material from both sides during machining.

The analysis of graphical trends from Fig. 11 and the demonstration in Fig. 12 have resulted that an increase in the Pf from level 1 (4 kg/cm²) to level 3 (12 kg/cm²) produces more KW from 0.354 mm to 0.366 mm on both sides of the workpiece. The reason is that the strong flushing leads to the removal of the debris particles at a faster rate; thus, more extra material is removed from both sides of the workpiece. Thus, KW is increased by increasing the Pf. The increase in nozzle size from 4 to 8 mm caused the increase of sparks gap among the two electrodes during machining. The enhancement in the spark gap increases the area of

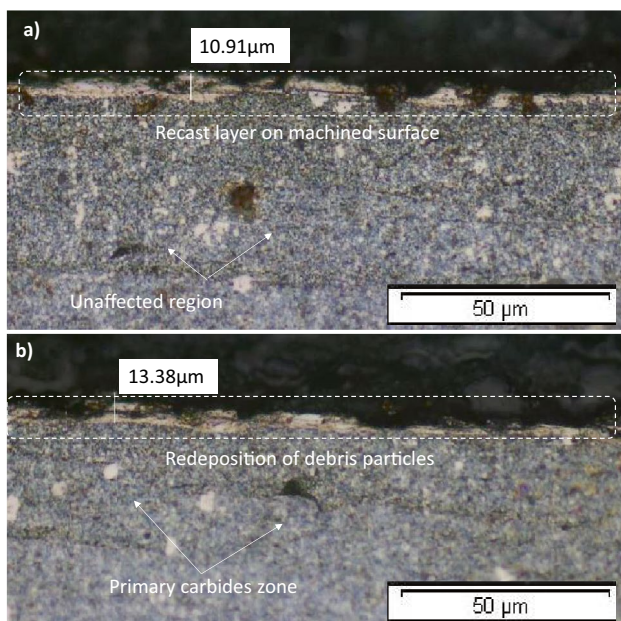
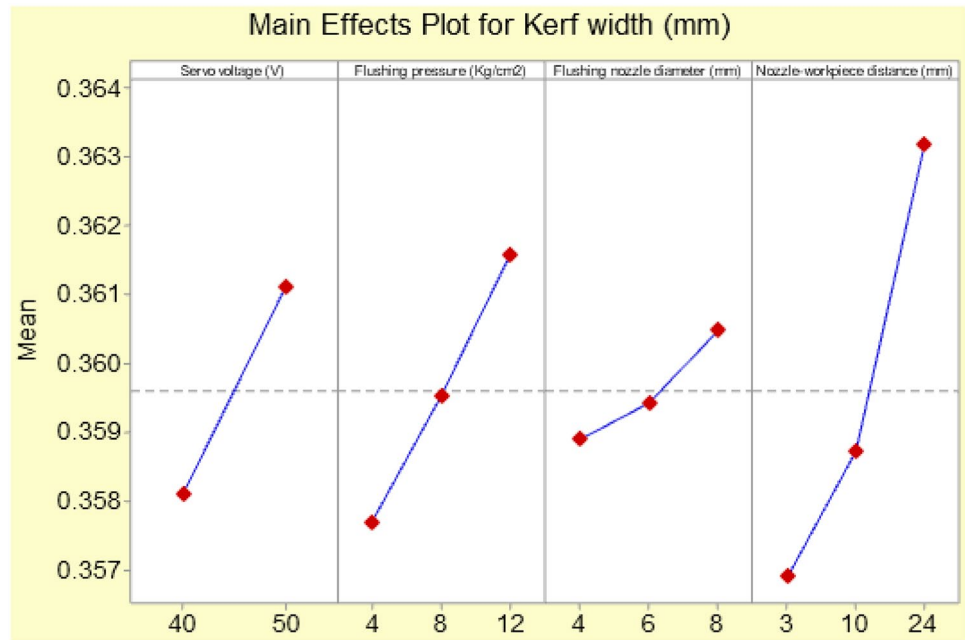


Fig. 10 Micrograph to analysis the RLT of machined surface for (a) 5th experiment, and (b) 12th experiment

Fig. 11 Graphical illustration to indicate the parametric influence of control variables for KW

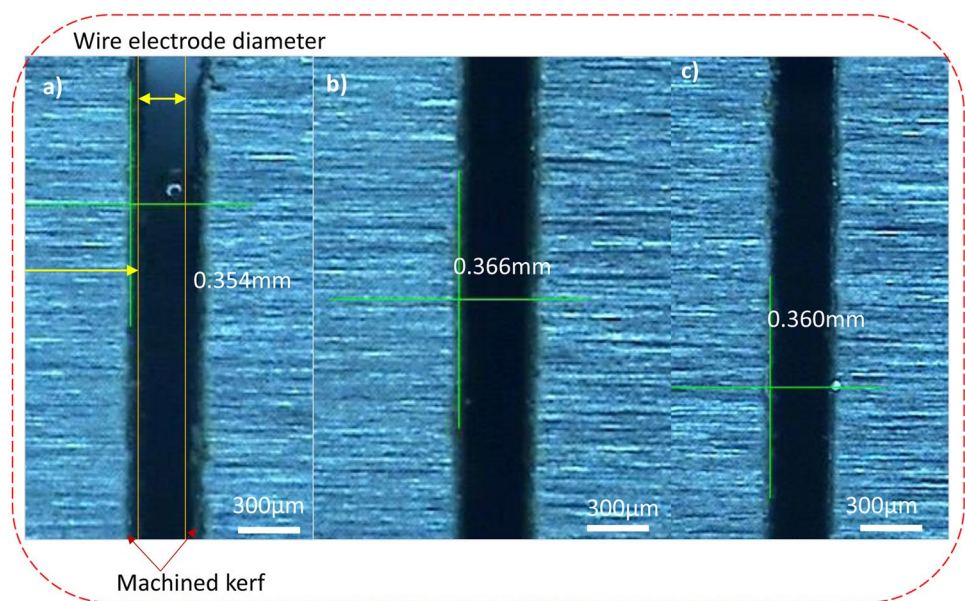


HAZ. Thus, the KW was increased by increasing the Dn. The results of graphical trends from Fig. 12 have proved that the large size nozzle (8 mm) will tend to produce a wider kerf (0.366 mm). Figure 14c produces the best results because kerf width is only 46 μm larger than the wire diameter (0.25 mm) with extremely smooth cut lines. The kerf width of 14a is smaller than b and d, but shows a lot of irregularities on the machined surface and should show deep craters and increased roughness.

The area of HAZ gets increased due to increased plasma energy by increasing the gap among the two

electrodes up to a controlled threshold limit. This increased HAZ damages more to the sides of the machined surface resulting in increased sparks gap during machining. Thus, the KW is increased from 0.354 mm to 0.366 mm by increasing d from 3 to 24 mm as evidenced in Fig. 12. Essentially, the existence of higher discharge energy pulses at the workpiece surface deteriorates the profile of the machined surface, and enhancing pulse duration increases the energy content of the pulses at high servo voltage, which influences the machined surface, and results in larger kerf width.

Fig. 12 Examination for the measurement of machined kerf after machining



3.2 Regression analysis

The key purpose of the regression analysis is the determination of the influencing control variables and their significance for output responses. There exist variations in actual and theoretical measurements. However, there exist standard deviations in the data. Thus, the regression-based numerical modeling is performed to cope with these variations by standardizing the data, determining the significance order of control variables, and the generation of the mathematical models for prediction as mentioned in Eqs. (2)–(4) for MRR, Ra, and KW. These regression equations may assist in the prediction of MRR, Ra, and KW.

$$MRR = 0.11851 + 0.001551Vs + 0.001869Pf - 0.005825Dn + 0.000946d \quad (2)$$

$$Ra = 1.7732 + 0.004222Vs - 0.01063Pf + 0.02333Dn - 0.001480d \quad (3)$$

$$KW = 0.33607 + 0.000301Vs + 0.000396Pf + 0.000396Dn + 0.000302d \quad (4)$$

3.2.1 Regression-based analysis of variance

The analysis of variance (ANOVA) approach is commonly used to determine the primary relevance of each control variable on the output response. It is a crucial technique for examining the significance of process factors by separating data observations into many responsible sources and assigning variation in components to control variables and noise [22]. Variance analysis was conducted at a confidence level of 95%. The parameters with a *P*-value less than 0.05 were designated as significant variables for a given response variable [23]. Table 4 shows the ANOVA's comprehensive results data. The parametric importance may also be stated using *F*-value, where a larger *F*-value indicates that a process parameter is more relevant for a certain output

response than other control variables [24]. It was found that the process variables like flushing nozzle diameter and nozzle workpiece distance influenced more for MRR, Ra, and Kw as followed by the flushing pressure and servo voltage.

An in-depth analysis of the observations from Table 4 has inferred that all the control variables were found significant for output responses. However, the nozzle workpiece distance (*d*) influenced more (53.86%), followed by the nozzle diameter (42.56%), and flushing pressure (35.30%). The nozzle diameter (*Dn*) was found a highly significant control variable for both MRR and SR with percentage contribution of 34.50% and 42.56%, respectively. However, it influenced the least (3.24%) for KW. It is due to the fact that when nozzle orifice area is increased, more dielectric escapes from flushing nozzle, and the intensity of dielectric flushing reduces according to the equation of continuity in fluids. The consistent intensity of sparks discharges on target surface is also reduced because of increased nozzle orifice. Therefore, the rate of flow of dielectric on KW is less affected whereas the MRR and SR are more affected by *Dn*. The control variable *Dn* was found highly significant for MRR with a percentage contribution of 34.50% followed by *d* (26.02%), *Vs* (22.94%), and *Pf* (14.21%), respectively. Similarly, the top influencing variables for Ra include *Dn* (42.56%), *Pf* (35.30%), *Vs* (13.07%), and *d* (4.89%). The nozzle workpiece distance was found highly significant throughout the analysis with PCR of 53.86% and followed by *Pf* (19.49%), *Vs* (17.58%), and *Dn* (3.24%), respectively. The regression summary reported in Table 5 has confirmed the statistical significance of the current study and the related descriptive statistics are mentioned in Table 6.

3.2.2 Analysis of Pareto and normal charts

The strength of the parametric effects for a certain response measure can be predicted with the help of Pareto charts whereas the closeness of statistical results from the

Table 4 Detailed variance analysis

Output response	MRR				Ra			KW		
	Source	DF	<i>F</i> -value	<i>P</i> -value	Contribution (%)	<i>F</i> -value	<i>P</i> -value	Contribution (%)	<i>F</i> -value	<i>P</i> -value
Regression	4	135.85	0.000	97.66	74.52	0.000	95.82	52.38	0.000	94.16
<i>Vs</i>	1	127.62	0.000	22.94	40.64	0.000	13.07	39.11	0.000	17.58
<i>Pf</i>	1	79.04	0.000	14.21	109.82	0.000	35.30	43.36	0.000	19.49
<i>Dn</i>	1	191.98	0.000	34.50	132.4	0.000	42.56	7.21	0.019	3.24
<i>d</i>	1	144.76	0.000	26.02	15.22	0.002	4.89	119.84	0.000	53.86
Error	13	–	–	2.34	–	–	4.18	–	–	5.84
Total	17	–	–	100	–	–	100	–	–	100

Table 5 Summary of the proposed regression analysis

Response	R-square	R-square (adjusted)	R-square (predicted)
MRR	97.66%	96.94%	95.31%
Ra	95.82%	94.54%	92.02%
Kw	94.16%	92.36%	89.31%

mean line values along with statistical deviations can be depicted in normal charts. The more significant process parameters for a specific response are obtained in the form of a pictorial representation as can be seen in Fig. 13.

The analysis of statistical data observations from Fig. 13a resulted that Dn, d, and Vs are the top influencing variables for MRR. The normal plots also depicted the closeness of readings with the mean line which infers the statistical significance of the control variables for MRR. The analysis of observations from the Pareto charts in Fig. 13b has indicated that the Dn and Pf are highly influential for Ra. The nozzle workpiece was found highly influential process variable for Kw as shown in Fig. 13c. Minor statistical deviations were found for all three aforesaid output responses which reveal the statistical significance of this study.

3.3 Parametric optimization

3.3.1 Mono-objective optimization

The signal to noise (S/N ratio) ratio analysis was used to generate the optimal settings in this study, which used single response parametric optimization. It helps to attain optimal settings for performing the confirmatory experimentation concerning the research validation [24]. Table 7 shows the S/N ratio data. For MRR, the larger the better approach was used; however, for Ra and Kw, the smaller the better relationship was used. Equations (5) and (6) are the mathematical relationships in S/N ratio analysis.

$$\eta_{ij} = -10\log\left[\frac{1}{n} \sum_{k=1}^n (Y_{ij}^2)\right] \tag{5}$$

$$\eta_{ij} = -10\log\left[\frac{1}{n} \sum_{k=1}^n \left(\frac{1}{Y_{ij}^2}\right)\right] \tag{6}$$

Table 6 Descriptive statistics of the regression analysis

Response	MRR			Ra			KW		
	SE Coef	95% CI	T-value	SE Coef	95% CI	T-value	SE Coef	95% CI	T-value
Vs	0.00014	(0.001254, 0.001848)	11.30	0.00066	(0.0027, 0.005)	6.38	0.00005	(0.000197, 0.000405)	6.25
Pf	0.00021	(0.001415, 0.002323)	8.89	0.00101	(-0.0128, -0.0084)	-10.5	0.00007	(0.000326, 0.000645)	6.59
Dn	0.00042	(-0.00673, -0.00491)	-13.9	0.00203	(0.01895, 0.02771)	11.51	0.00015	(0.000077, 0.000714)	2.68
d	0.00008	(0.000776, 0.001116)	12.03	0.00038	(-0.0022, -0.0006)	-3.90	0.00003	(0.000242, 0.000361)	10.95

where Y_{ij} is the average output value and n denotes the number of completed repetitions. In Table 7, the process parameter with the greatest potential for influence is ranked first. Confirmation trials, the results of which are listed in Table 7, have also been used to verify the hypothesized best combination.

The results from Table 8 have highlighted the supremacy of flushing characteristics for MRR (9.877%), followed by Ra (7.163%), and Kw (4.425%), by performing confirmatory experiments with parametric combinations (Vs2, Pf3, Dn1, d3), (Vs1, Pf3, Dn1, d3), and (Vs1, Pf1, Dn1, d1), respectively.

3.3.2 Gray rational analysis-based multi-objective optimization

Gray rational analysis (GRA) is an effective statistical technique for multi-objective optimization of conflicting responses. It can analyze the multiple variables simultaneously and reduce the deficiencies of the statistical analysis. Generally, the sequence of original response results is normalized between 0 and 1 by using three distinct normalizing relations such as (i) higher the better, (ii) nominal the best, and (iii) lower the better (Eqs. (7)–(9)) used depending upon the nature of desired response [25].

$$\text{Higher the better } X_{ij} = \frac{Y_{ij} - (Y_{ij})_{min}}{(Y_{ij})_{max} - (Y_{ij})_{min}} \tag{7}$$

$$\text{Nominal the best } X_{ij} = 1 - \frac{|Y_{ij} - Y|}{(\beta_{ij})_{max} - \beta} \tag{8}$$

$$\text{Lower the better } X_{ij} = \frac{(Y_{ij})_{max} - Y_{ij}}{(Y_{ij})_{max} - (Y_{ij})_{min}} \tag{9}$$

where X_{ij} is the normalized measure of j th experiment in the i th sequence, while Y_{ij} is the i th response value of the j th experiment, and Y is the targeted output measure. Higher the better function is desirable for MRR, while lower the better normalization relation is preferred in the case of Kw and Ra.

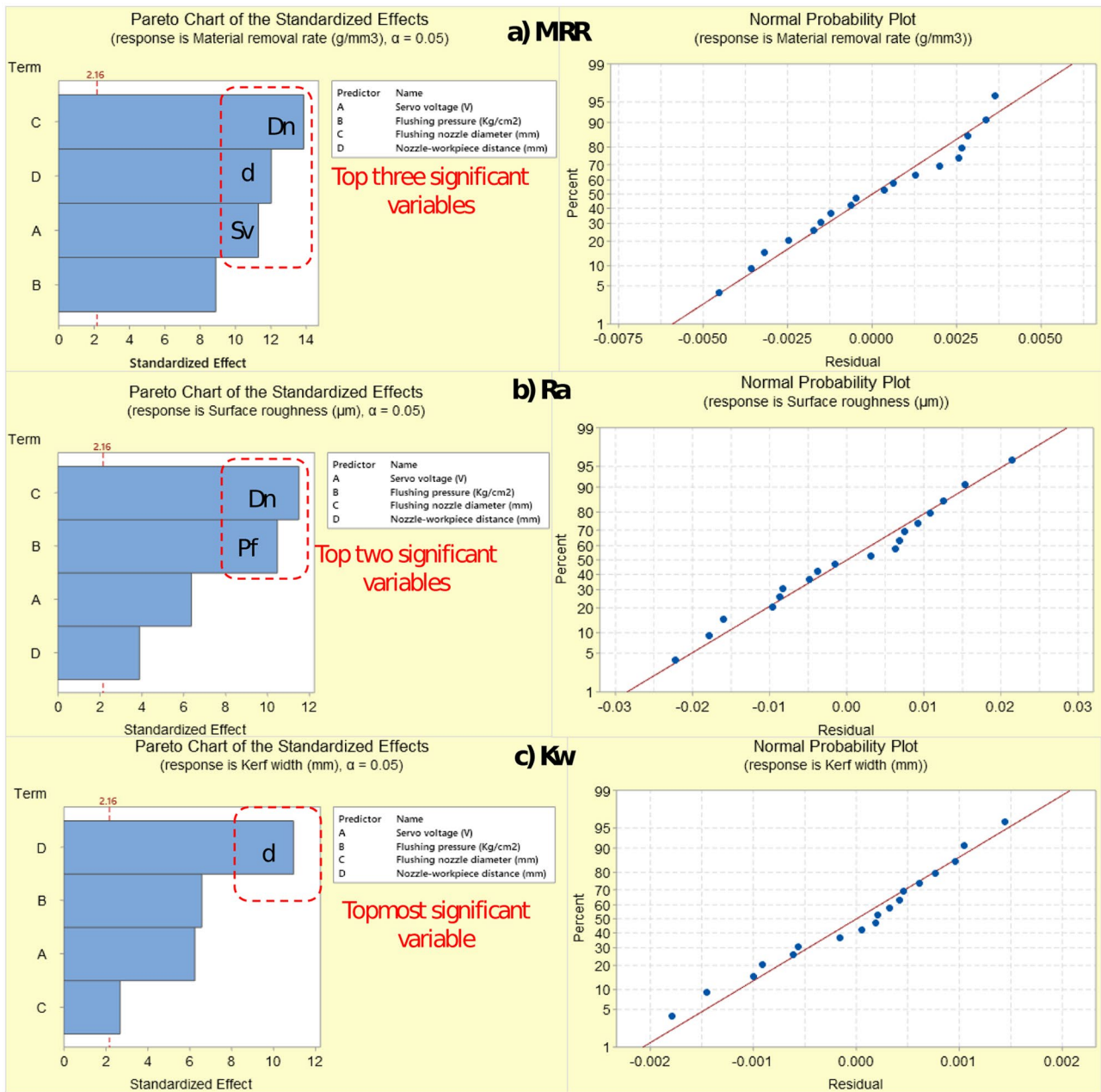


Fig. 13 Graphical illustration to show the Pareto and normal plots for (a) MRR, (b) Ra, and (c) KW

Gray relational coefficient (GRC) is used to determine the correlation between normalized and optimum response values. GRC was calculated by using Eq. (10):

$$\gamma_{ij} = \frac{(\Delta)_{\min} + \xi(\Delta)_{\max}}{\Delta_{ij} + \xi(\Delta)_{\max}} \quad (10)$$

where γ_{ij} is the GRC of the i th normalized measure of the j th experiment. ξ is the differentiating coefficient and generally its value is selected between 0 and 1. In current research work, the value of ξ is chosen 0.5. Δ_{\min} and Δ_{\max}

are the minimum and maximum absolute deviations from the targeted value, while Δ_{ij} is the deviation sequence which determines the deviance of normalized measure from the ideal value of 1. These deviations are expressed as in Eqs. (11)–(13) [25]:

$$\Delta_{\max} = \max_i \max_j (y_i^o - y_{ij}) \quad (11)$$

$$\Delta_{\min} = \min_i \min_j (y_i^o - y_{ij}) \quad (12)$$

$$\Delta_{ij} = (y_i^o - y_{ij}) \quad (13)$$

Table 7 Detailed results for the signal to noise ratio

(a) MRR						
Factor	L1	L2	L3	Delta	Ranking	
Vs	-15.29	-14.57		0.73	3	
Pf	-15.31	-14.89	-14.59	0.72	4	
Dn	-14.4	-14.89	-15.5	1.09	1	
d	-15.28	-15.11	-14.4	0.88	2	
(b) Ra						
Factor	L1	L2	L3	Delta	Ranking	
Vs	-5.926	-6.108		0.182	3	
Pf	-6.226	-5.967	-5.858	0.368	2	
Dn	-5.814	-6.018	-6.219	0.405	1	
d	-6.097	-6.001	-5.953	0.144	4	
(c) Kw						
Factor	L1	L2	L3	Delta	Ranking	
Vs	8.92	8.848		0.073	3	
Pf	8.93	8.886	8.836	0.094	2	
Dn	8.901	8.888	8.862	0.039	4	
d	8.949	8.905	8.798	0.152	1	

Table 8 Detailed data for confirmatory experimentation

Response measures	DOE data		SN ratio data			% improvement from DOE results
	Un-optimized settings	Response values	Optimized settings	Predicted results based on DOE	Confirmatory experiments results	
MRR (g/mm ³)	Vs2,Pf3, Dn1, d3	0.2199	Vs2,Pf3, Dn1, d3	0.2179	0.244	9.870
Ra (µm)	Vs1,Pf3, Dn1, d2	1.9	Vs1,Pf3, Dn1,d3	1.8805	1.773	7.163
Kw (mm)	Vs1,Pf1, Dn1, d1	0.354	Vs1,Pf1, Dn1, d1	0.3527	0.339	4.425

Table 9 Multi-objective optimization using gray rational analysis

Exp. No.	Normalizing sequence			Deviation sequence			Gray relational coefficient			Gray relational grade (GRG)	Rank
	MRR	Ra	Kw	MRR	Ra	Kw	MRR	Ra	Kw		
1	0.0552	0.5000	1.0000	0.9448	0.5000	0.0000	0.3461	0.5000	1.0000	0.6154	4
2	0.0000	0.4545	0.7951	1.0000	0.5455	0.2049	0.3333	0.4783	0.7093	0.5070	11
3	0.0121	0.2727	0.4426	0.9879	0.7273	0.5574	0.3360	0.4074	0.4729	0.4054	18
4	0.2328	0.8636	0.9426	0.7672	0.1364	0.0574	0.3946	0.7857	0.8971	0.6924	2
5	0.1845	0.7273	0.8689	0.8155	0.2727	0.1311	0.3801	0.6471	0.7922	0.6064	5
6	0.1897	0.5455	0.2951	0.8103	0.4545	0.7049	0.3816	0.5238	0.4150	0.4401	14
7	0.4397	1.0000	0.6230	0.5603	0.0000	0.3770	0.4715	1.0000	0.5701	0.6805	3
8	0.4759	0.8636	0.2623	0.5241	0.1364	0.7377	0.4882	0.7857	0.4040	0.5593	8
9	0.0121	0.5455	0.7459	0.9879	0.4545	0.2541	0.3360	0.5238	0.6630	0.5076	10
10	0.7707	0.5909	0.4344	0.2293	0.4091	0.5656	0.6856	0.5500	0.4692	0.5683	7
11	0.2103	0.1364	0.9262	0.7897	0.8636	0.0738	0.3877	0.3667	0.8714	0.5419	9
12	0.0224	0.0000	0.5820	0.9776	1.0000	0.4180	0.3384	0.3333	0.5446	0.4055	17
13	0.5466	0.7273	0.5902	0.4534	0.2727	0.4098	0.5244	0.6471	0.5495	0.5737	6
14	0.6276	0.5455	0.0492	0.3724	0.4545	0.9508	0.5731	0.5238	0.3446	0.4805	13
15	0.1414	0.1818	0.5328	0.8586	0.8182	0.4672	0.3680	0.3793	0.5169	0.4214	16
16	1.0000	0.8636	0.0000	0.0000	0.1364	1.0000	1.0000	0.7857	0.3333	0.7063	1
17	0.4328	0.5455	0.4262	0.5672	0.4545	0.5738	0.4685	0.5238	0.4656	0.4860	12
18	0.2569	0.4545	0.2131	0.7431	0.5455	0.7869	0.4022	0.4783	0.3885	0.4230	15

Table 10 ANOVA of GRG

Source	DF	Seq SS	Contribution	Adj SS	Adj MS	F-value	P-value
Regression	4	0.145353	88.08%	0.145353	0.036338	24.02	0.000
Servo voltage	1	0.009225	5.59%	0.009225	0.009225	6.10	0.028
Flushing pressure	1	0.008491	5.15%	0.008491	0.008491	5.61	0.034
Nozzle diameter	1	0.126814	76.85%	0.126814	0.126814	83.83	0.000
Nozzle workpiece distance	1	0.000823	0.50%	0.000823	0.000823	0.54	0.474
Error	13	0.019665	11.92%	0.019665	0.001513		
Total	17	0.165018	100.00%				
Std dev	R-sq	R-sq(adj)	PRESS	R-sq(pred)			
0.0388933	88.08%	84.42%	0.0387772	76.50%			

Fig. 14 Main effects plot for GRG

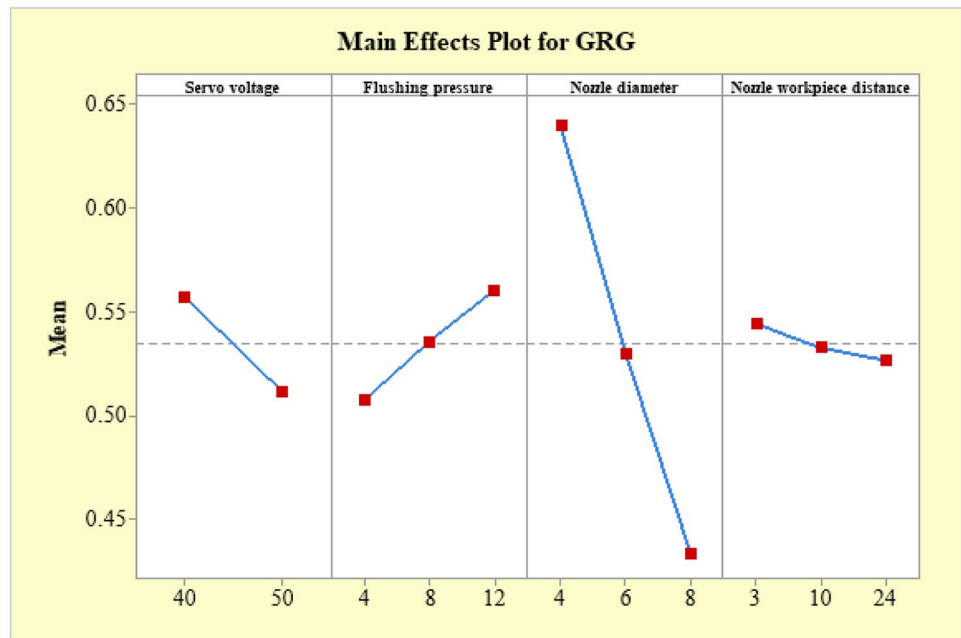


Table 11 Response table for GRG

Level	Servo voltage	Flushing pressure	Nozzle diameter	Nozzle workpiece distance
1	0.5571	0.5072	0.6394	0.5441
2	0.5118	0.5358	0.5302	0.5327
3	-	0.5605	0.4338	0.5266
Delta	0.0453	0.0532	0.2056	0.0175
Rank	3	2	1	4

Gray rational grade (GRG) is the weighting sum of all GRC. It is calculated by using Eq. (14):

$$\delta_j = \frac{1}{n} \sum_{i=1}^n \gamma_{ij} \tag{14}$$

where δ_j denotes the GRG of j th experiment and n represents the number of responses. The value of GRG varies from 1 to 0, while the highest GRG value infers the optimal set of process parameters for all responses simultaneously and ranked as 1st. Table 9 presents the gray relational analysis calculations for multi-objective optimization for conflicting responses.

From Table 9, it is clear that the highest GRG value of experiment number 16 is 1 which ranked 1st. This depicts those optimum results of MRR, Ra, and Kw can be attained simultaneously at optimal parametric conditions of Vs = 50 V, Pf = 12 kg/cm², Dn = 11 mm, and d = 24 mm.

To find the most significant process parameters, ANOVA is also performed for GRG values after the ranking. It can be noted from Table 10 that Vs, Pf, and Dn are significant for GRG, with a P-value less than 0.05. The percentage contribution for Dn is 76.85%, while for Vs and Pf it is 5.59%

and 5.15%, respectively. The main effect plot for GRG is illustrated in Fig. 14. The response table (Table 11) shows the levels resulting in the highest GRG values. Vs, Dn, and d at level 1 while Pf at level 3 shows the highest GRG.

4 Conclusions

The industry anticipates technological advancements for productivity improvement, and this can be accomplished by improving the machining performance in the areas where machinability challenges exist. The machinability and productivity of wire electric discharge machining (WEDM), which is a popular non-conventional cutting process, can be improved while having comparable surface integrity. Previously the non-conventional machining literature is focused on the machinability investigations of various industrial materials and process optimization. However, no extensive research on the study of flushing parameters optimization to improve machinability in non-conventional machining is known. In this research, WEDM of M42 HSS using controlled flushing is performed resulting in improved machinability in terms of material removal rate (MRR), surface roughness (Ra), and kerf width (KW). The conclusions drawn from the research include:

- The flushing nozzle diameter also plays its part in influencing MRR. According to the equation of continuity for the fluids, the less is the orifice area, the more will be the flushing speed. Therefore, a linear decrease in MRR was obtained from 21.9 mm³/min to 16.2 mm³/min by increasing the Dn from level 1 (4 mm) to level 3 (8 mm).
- Greater magnitudes of flushing pressure and nozzle diameter boost MRR and surface finish. All the control variables namely nozzle diameter, servo voltage, flushing pressure, and nozzle-workpiece distance showed linear effect with kerf width.
- The topographical examination indicated that Pf causes the reduction in crater size (depth and width), and the redeposition of debris particles on the machined surface to enhance the MRR and surface finish.
- Multi-response optimization was also performed and depicts the possibility of achieving optimized values of MRR, Ra, and, KW simultaneously. Mono-objective optimization by confirmatory experimentation provided a higher MRR (9.877%), along with least Ra (7.163%), and Kw (4.425%), at optimal settings (Vs2, Pf3, Dn1, d3), (Vs1, Pf3, Dn1, d3), and (Vs1, Pf1, Dn1, d1), respectively. The gray rational analysis-based multi-response optimization produced an optimal parametric setting for controlled lubrication-based machining as (Vs1, Pf3, Dn1, d1) optimizing all responses simultaneously.

- The findings indicate that the nozzle diameter (76.85%) has a substantial influence on total machining performance. Nozzle diameter, nozzle-workpiece distance, servo voltage, and flushing pressure all had a substantial influence on MRR, with percentage contributions of 34.50%, 26.02%, 22.94%, and 14.21%, respectively. The processing variables for Ra followed the influential sequence as Dn (42.56%), Pf (35.30%), Vs (13.07%), and d (4.89%), correspondingly. The KW was highly affected by d (53.86%) followed by Pf (19.49%), Vs (17.58%), and Dn (3.24%), respectively.
- The evaluation of output responses resulted in an increased MRR (21.99 mm³/min), along with reduced Ra (1.90 μm), and Kw (0.354 mm), respectively. Higher levels of ‘Pf’ and ‘d’ are observed to enhance the machining performance in terms of improved MRR and surface finish. The rationale of this improvement is the easy evacuation of debris particles from the working regime.
- The flush-controlled machining improved work quality in terms of accurate production, increased productivity by lowering process time, and improved surface integrity of the machined piece thus can be a possible process advancement in the aerospace and automotive industries.

Author contribution Sana Ehsan: conceptualization, data collection, validation; Mudassar Rehman: writing—original draft, data analysis, visualization; Muhammad Umar Farooq: writing—original draft, data analysis, visualization, editing and review; Muhammad Asad Ali: software, data analysis, editing and review; Mohammad Pervez Mughal: conceptualization, supervision, resources.

Data availability All the concerned data are already contained in the paper.

Declarations

Ethics approval The authors confirm that they have abided by the publication ethics and state the originality of this work which has not been used anywhere else for publication.

Consent to publish The authors allow the publishing of this work.

Competing interests The authors declare no competing interests.

References

1. Haq MA, Hussain S, Ali MA, Farooq MU, Mufti NA, Pruncu CI, Wasim A (2021) Evaluating the effects of nano-fluids based MQL milling of IN718 associated to sustainable productions. *J Clean Prod* 310:127463. <https://doi.org/10.1016/j.jclepro.2021.127463>
2. Singh RP, Singh R, Trehan R, Garg RK, Tyagi M (2021) Investigation into the surface quality in wire-cut EDM of M42 HSS: an experimental study and modeling using RSM. *Optim Methods Eng Springer* 245–256

3. Singh R, Singh RP, Tyagi M, Kataria R (2019) Investigation of dimensional deviation in wire EDM of M42 HSS using cryogenically treated brass wire. *Mater Today Proc* 25:679–685. <https://doi.org/10.1016/j.matpr.2019.08.028>
4. Prathipati R, Dora SP, Chanamala R (2020) Wear behavior of wire electric discharge machined surface of 316L stainless steel. *SN Appl Sci* 2:1–8. <https://doi.org/10.1007/s42452-020-2244-z>
5. Qudeiri JEA, Zaiout A, Mourad A-HI, Abidi MH, Elkaseer A (2020) Principles and characteristics of different EDM processes in machining tool and die steels. *Appl Sci (Switzerland)* 10:1–46. <https://doi.org/10.3390/app10062082>
6. Singaravel B, Shekar KC, Reddy GG, Prasad SD (2020) Experimental investigation of vegetable oil as dielectric fluid in electric discharge machining of Ti-6Al-4V. *Ain Shams Eng J* 11:143–147. <https://doi.org/10.1016/j.asej.2019.07.010>
7. Chakraborty S, Mitra S, Bose D (2020) Experimental investigation on enhancing die corner accuracy during powder mixed wire EDM of Ti6Al4V. *Mater Today Proc* 38:3097–3102. <https://doi.org/10.1016/j.matpr.2020.09.491>
8. Pramanik A, Islam MN, Basak AK, Dong Y, Littlefair G, Prakash C (2019) Optimizing dimensional accuracy of titanium alloy features produced by wire electrical discharge machining. *Mater Manuf Processes* 1–8. <https://doi.org/10.1080/10426914.2019.1628259>
9. Nayak I, Rana J (2020) Precision multi-response optimization of performance characteristics in wire-cut electric discharge machining (WEDM) process. *J Mech Eng* 17:39–54
10. Rehman M, Khan SA, Naveed R (2020) Parametric optimization in wire electric discharge machining of DC53 steel using gamma phase coated wire. *J Mech Sci Technol* 34:2767–2773. <https://doi.org/10.1007/s12206-020-0609-2>
11. Singh R, Singh RP, Tyagi M, Kataria R (2020) Investigation of dimensional deviation in wire EDM of M42 HSS using cryogenically treated brass wire. *Mater Today Proc* 25:679–685
12. Camposeco-Negrete C (2019) Prediction and optimization of machining time and surface roughness of AISI O1 tool steel in wire-cut EDM using robust design and desirability approach. *Int J Adv Manuf Technol* 103:2411–2422. <https://doi.org/10.1007/s00170-019-03720-3>
13. Straka E, Dittrich G (2020) Influence of tool steel properties on surface quality after electrical discharge machining by wire electrode. *Int J Adv Manuf Technol* 106:1617–1632
14. Sanke N (2021) Evaluation of tensile and microstructure properties of AA2014 and AA7075 FSW weldments developed by HSS-10% Co and WC tools. *Mater Today Proc*
15. Ar J, Balasubramanian K, Palanisamy D, AGS E, (2020) Experimental investigations on WEDM process for machining High Manganese steel. *Mater Manuf Processes* 00:1–10. <https://doi.org/10.1080/10426914.2020.1779941>
16. Kumar V, Kharub M, Kumar R, Rakesh PK (2021) Process parameters optimization of wire EDM on AISI 304 using the Taguchi method. *Adv Eng Des Springer* 363–371
17. Efendee AM, Azhari A, Hasnain AR, Ariffin SZ, Mukhtar M (2021) Investigation of magnetic field effect on MRR, EWR and surface roughness during EDM of AISI420 tool Steel. In IOP Conference Series: Materials Science and Engineering. IOP Publishing 12018
18. Patel Gowdru Chandrashekarappa M, Kumar S, Jagadish, Pimenov DY, Giasin K (2021) Experimental Analysis and Optimization of EDM Parameters on HcHcr Steel in Context with Different Electrodes and Dielectric Fluids Using Hybrid Taguchi-Based PCA-Utility and CRITIC-Utility Approaches. *Metals* 11:419. <https://doi.org/10.3390/met11030419>
19. Wang W, Qiu M, Liu Z, Zhang M, Shao C (2020) Study on the influence of kerosene content on burn in high speed–wire cut electrical discharge machining dielectric fluid. *Int J Adv Manuf Technol* 107:3135–3143. <https://doi.org/10.1007/s00170-020-05187-z>
20. Khan SA, Rehman M, Farooq MU, Ali MA, Naveed R, Pruncu CI, Ahmad W (2021) A detailed machinability assessment of DC53 steel for die and mold industry through wire electric discharge machining. *Metals* 11:816. <https://doi.org/10.3390/met11050816>
21. Wu X, Li S, Jia Z, Xin B, Yin X (2019) Using WECM to remove the recast layer and reduce the surface roughness of WEDM surface. *J Mater Process Technol* 268:140–148
22. Dehghan S, Soury E, Ismail MIS, b. (2021) A comparative study on machining and tool performance in friction drilling of difficult-to-machine materials AISI304, Ti-6Al-4V, Inconel718. *J Manuf Process* 61:128–152. <https://doi.org/10.1016/j.jmapro.2020.10.078>
23. Ramesh S, Jenarathanan MP (2021) Optimizing the powder mixed EDM process of nickel based super alloy. *Proc Inst Mech Eng Part E J Process Mech Eng.* <https://doi.org/10.1177/09544089211002782>
24. Sharma S, Kumar Vates U, Bansal A (2020) Parametric optimization in wire EDM of D2 tool steel using Taguchi method. *Mater Today Proc.* <https://doi.org/10.1016/j.matpr.2020.02.802>
25. Kuram E, Ozcelik B (2013) Multi-objective optimization using Taguchi based grey relational analysis for micro-milling of Al 7075 material with ball nose end mill. *Measurement* 46:1849–1864
26. Ishfaq K, Farooq MU, Pruncu CI (2021) Reducing the geometrical machining errors incurred during die repair and maintenance through electric discharge machining (EDM). *Int J Adv Manuf Technol* 117(9–10):3153–3168. <https://doi.org/10.1007/s00170-021-07846-1>
27. Ishfaq K, Farooq MU, Anwar S, Ali MA, Ahmad S, Ahmed, M, El-Sherbeeny A (2021) A comprehensive investigation of geometrical accuracy errors during WEDM of Al6061-7.5%SiC composite. *Mater Manuf Process* 36(3):362–372. <https://doi.org/10.1080/10426914.2020.1832683>
28. Farooq MU, Ali MA, He Y, Khan AM, Pruncu CI, Kashif M, Ahmed N, Asif N (2020) Curved profiles machining of Ti6Al4V alloy through WEDM: investigations on geometrical errors. *J Mater Res Technol* 9(6):16186–16201. <https://doi.org/10.1016/j.jmrt.2020.11.067>
29. ASTM (2021) Material directory. <https://www.astmsteel.com/product/m2-tool-steel-1-3343-hs-6-5-2c-sk51/> (accessed Aug 01, 2021)

Publisher's note Springer Nature remains neutral with regard to jurisdictional claims in published maps and institutional affiliations.